crystals

MDPI

Article

Micro-Vickers Hardness of Cu and Cu_2O Dual Phase Composite Films Electrodeposited from Acidic Aqueous Solutions Containing Polyethylene Glycol

Reina Kawakami [1], Ryusei Saeki [2], Shinji Munetoh [2] and Takeshi Ohgai [3,*]

[1] Graduate School of Engineering, Nagasaki University, 1-14 Bunkyo-machi, Nagasaki 852-8521, Japan; bb52122615@ms.nagasaki-u.ac.jp
[2] Faculty of Engineering, Kyushu University, 744 Motooka, Nishi-ku, Fukuoka 819-0395, Japan; saeki.ryusei.719@m.kyushu-u.ac.jp (R.S.); munetoh.shinji.599@m.kyushu-u.ac.jp (S.M.)
[3] Faculty of Engineering, Nagasaki University, 1-14 Bunkyo-machi, Nagasaki 852-8521, Japan
* Correspondence: ohgai@nagasaki-u.ac.jp; Tel.: +81-95-819-2638

Abstract: Metallic copper (Cu) and copper oxide (Cu_2O) dual phase composite films were fabricated via a cathodic reduction process in an acidic aqueous solution dissolving polyethylene glycol (PEG) to investigate the structure and micro-Vickers hardness. By dissolving PEG in an aqueous electrolyte, the cathode potential was depolarized to the noble region during the electrodeposition, and the average crystallite size of electrodeposited Cu/Cu_2O composite films was decreased down to around 40 nm. The metallic copper films electrodeposited from the solution without PEG was preferentially orientated in (220), while that containing PEG was composed of Cu and Cu_2O dual phase composite films with random crystal orientation. The micro-Vickers hardness of the Cu/Cu_2O composite films that were electrodeposited from the solution containing PEG was achieved up to 2.53 GPa. This improvement in mechanical performance can be explained by the grain refinement effect and the electrochemical phase transformation effect from a copper metallic state to the oxide.

Keywords: electrodeposition; copper; copper oxide; composite film; polyethylene glycol; crystal grain refinement; micro-Vickers hardness

check for updates

Citation: Kawakami, R.; Saeki, R.; Munetoh, S.; Ohgai, T. Micro-Vickers Hardness of Cu and Cu_2O Dual Phase Composite Films Electrodeposited from Acidic Aqueous Solutions Containing Polyethylene Glycol. *Crystals* **2023**, *13*, 1654. https://doi.org/10.3390/cryst13121654

Academic Editor: Shouxun Ji

Received: 24 October 2023
Revised: 20 November 2023
Accepted: 28 November 2023
Published: 30 November 2023

1. Introduction

Metal oxide semiconductors such as In_2O_3, SnO_2, Ga_2O_3, ZnO, Cu_2O and their compounds have been investigated so far [1,2]. For example, Kimizuka et al. succeeded in synthesizing the $InGaZnO_4$ (IGZO) crystals in 1985 [3], and Hosono et al. developed IGZO thin-film transistors as a backplane material in a flat-panel display [4,5]. Recently, Cu_2O has been of interest because of its diverse properties in regard to microstructure, electron transportation and optical absorption [6–8]. Cu_2O is widely used mainly in photovoltaic cells [9], sensor devices [10,11] and electronic devices [12]. Thin copper oxide films can be prepared by electrochemical deposition, thermal oxidation [13,14], chemical deposition [15] and sputtering [16]. Among them, the electrochemical cathodic reduction process is an attractive technique for preparing thin films and multilayers of metallic [17,18] and oxide semiconductors [19,20] on conductive substrates. This technology has several advantages in cost-effective operating conditions such as room temperature, atmospheric pressure and film growth rate. In addition, electrochemical deposition is highly dependent on electrodeposition conditions such as current density, pH [21], electrolyte composition, temperature [22,23], deposition time [24] and substrate characteristics [25]. Therefore, varying the electrolytic conditions can facilitate the development of Cu_2O morphology, structural properties and high-performance devices tailored to specific functional materials by controlling surface structure and mechanical properties. For example, adding an additive such as PEG to the plating solution will refine the electrodeposited crystal grains,

smoothing the surface and increasing micro-Vickers hardness [26]. In addition, the use of PEG as an additive is expected to produce Cu and Cu_2O dual phase composite films. Researchers have investigated the effects of the electrolytic deposition of copper oxide. In 1998, Zhou et al. studied the effect of pH on the electrolytic deposition of copper oxide [27]. They found that the electrochemical reactions during the cathodic reduction of copper (II) lactate solution and metallic Cu can be produced in the pH range less than 7. In 2007, Wang et al. studied the effect of pH on the crystallographic plane orientation [28]. They revealed that the (111) plane was preferentially oriented when the solution pH increased up to 12 from 9. PEG adsorption on the cathode will inhibit the diffusion of Cu atoms on the cathode. This PEG effect will inhibit the crystal growth of electrodeposited Cu and will induce the grain refinement of electrodeposits. Thus, the hardness of Cu and Cu_2O dual phase composite films which are electrodeposited from the solution dissolving PEG will be improved by the grain refinement effect and the oxide particles dispersion effect. Many researchers have reported on the fundamental properties, such as electron transportation and optical absorption of Cu_2O films [6–12]. On the contrary, mechanical properties such as hardness and tensile strength of Cu_2O films have not been clarified yet. If some mechanical stresses are introduced in Cu_2O films, some micro-cracks will easily occur in the film structures and will cause some harmful effects on the physical properties. Therefore, in the present study, Cu and Cu_2O dual phase composite films were prepared by a cathodic reduction process in an aqueous solution dissolving PEG, and their crystal texture and mechanical properties were also investigated.

2. Materials and Methods

An aqueous solution containing $CuSO_4{\cdot}5H_2O$ (1 M), H_3BO_3 (0.4 M) and PEG (Mw = 3000) (0.01–0.05 g/L) was synthesized as an electrolytic bath. Here, H_3BO_3 was added as a pH buffer to inhibit the pH rising in the vicinity of the cathode during the electrodeposition. The solution pH was around 3.5 by dissolving the above chemicals into an ultra-pure water solution. Hence, the solution pH was adjusted to 3.0 by adding an acidic aqueous solution containing H_2SO_4 (0.1 M). The solution temperature was kept to 40 °C. During the electrodeposition, the aqueous solutions were stirred at a speed of 300 rpm. A dumbbell-shaped metallic titanium, a metallic copper and a silver/silver chloride single junction electrode were utilized as a template cathode, a soluble anode and a standard reference electrode, respectively. Cu and Cu_2O dual phase composite films were electrodeposited by a galvanostatic mode at a current density of 900 A/m^2 for 10,532 s (around 3 h). The film thickness was controlled to be the range from 200 μm to 250 μm. For comparison, pure copper film was also electrochemically synthesized in an aqueous solution without dissolving PEG. After the electrodeposition, the dual phase composite films were exfoliated from the metallic titanium cathode to avoid the effect of substrate when we determined the structure and physical properties of the electrodeposited films. The film thickness was measured by a digital micrometer, MDC-25MJ (Mitutoyo, Kanagawa, Japan). The morphology of the dual phase composite films was examined using a scanning electron microscope (SEM), JCM-5700 (JEOL Ltd., Tokyo, Japan). The roughness of the samples R_a was determined by utilizing a stylus-type surface roughness tester, SURFTEST, SJ-210 (Mitutoyo, Japan). The crystal structure of the dual phase composite films was determined using an X-ray diffractometer, XRD, Miniflex600-DX (Rigaku Corp., Tokyo, Japan). Furthermore, their hardness was examined using a micro-Vickers hardness testing machine, HM-211 (Mitutoyo, Japan). During the measurement, the applied load was adjusted to 100 gf (0.98 N) and the dwell time was fixed to 10 s. It is well known that the hardness value of a casted and rolled copper sheet is about 1.08 GPa. In the above measurement condition, the indentation depth and the diagonal length are estimated to be around 5.9 μm and 41 μm, respectively. To avoid the effect of substrate, the sample thickness should be more than 10 times the indentation depth. Hence, in the above measurement condition, the sample thickness should be more than 59 μm. In the present study, to obtain the reliable hardness value, the film thickness was controlled to be the range from 200 μm to 250 μm.

3. Results and Discussion

3.1. Cathodic Polarization Behavior during Cu and Cu_2O Dual Phase Composite Electrodeposition

Prior to the electrodeposition of Cu and Cu_2O dual phase composite films, the cathodic polarization curves for the solutions without PEG (PEG-free) and containing PEG (PEG-addition) were plotted to determine the optimal electrolysis conditions, as shown in Figure 1. The cathode potential was swept from +0.20 V to −1.50 V vs. Ag/AgCl at a scan rate of 100 mVs^{-1}. The cathodic polarization curve that was obtained from the solution containing PEG was slightly depolarized to the noble direction than that without PEG. According to Nernst's equation, the equilibrium potential of Cu/Cu^{2+} (E_{cu}^{eq}) can be estimated as 0.140 V vs. Ag/AgCl based on the bath temperature and Cu^{2+} ion concentration (40 °C, $[Cu^{2+}]$ = 1 M). Here, the standard electrode potential of Cu/Cu^{2+} $\left(E_{cu}^{0} : Cu^{2+} + 2e^{-2} \leftrightarrows Cu\right)$ = 0.140 V vs. Ag/AgCl, the gas constant R = 8.3 J K^{-1} mol^{-1}, the solution temperature T = 313 K, the valence number of Cu^{2+} ions n = 2, the Faraday constant F = 96,485 C mol^{-1} and $[Cu^{2+}]/[Cu^{0}]$ = 1. As shown in the cathodic polarization curve that was obtained from the solution without PEG, the cathode current density sharply increased at the cathode potential of ca. 0.14 V vs. Ag/AgCl [29,30]. Considering the equilibrium potential of Cu/Cu^{2+}, the increase in the current density at ca. 0.14 V seems to be caused by the reduction of the Cu^{2+} ions. On the other hand, in the case of the polarization curve that was obtained from the solution containing PEG, the cathode current density began to increase at the cathode potential of ca. 0.11 V vs. Ag/AgCl. Based on the potential-pH diagram of the Cu^{2+}-H_2O system [31,32], the Cu^{2+} ions can form cuprous oxide (Cu_2O) at a cathode potential region nobler than the equilibrium potential of Cu/Cu^{2+}. This reaction can be expressed by using the following Equation (1). The cuprous oxide can be electrochemically reduced to metallic copper when pH of the electrolytic solution is less than 7 (pH < 7), as expressed by the following Equation (2) [27,33].

$$2Cu^{2+} + 2e^{-1} + H_2O \leftrightarrows Cu_2O + 2H^{+} \quad (1)$$

$$Cu_2O + 2e^{-1} + 2H^{+} \leftrightarrows 2Cu + H_2O \quad (2)$$

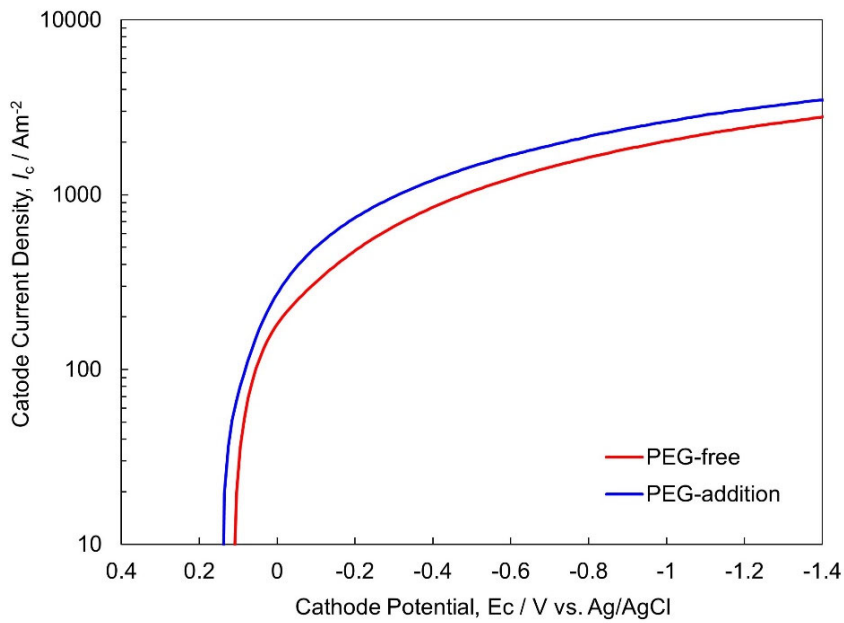

Figure 1. Effect of PEG addition on the cathodic polarization curves during the electrodeposition of Cu and Cu_2O dual phase composite films.

Generally, pH in the vicinity of the cathode rises due to the hydrogen evolution as a side reaction of electrodeposition. Boric acid added to the electrolytic solution can

suppress the increase in pH on the cathode (i.e., the pH buffering effect). Some polymers and surfactants (e.g., polyethylene glycol, gelatin) can adsorb to the electrode surface to form a layer and suppress the electrodeposition of metals [34,35]. As we will discuss later, the films that electrodeposited from the solution containing PEG had a Cu and Cu_2O dual phase composite structure. If the electrochemical reactions as described in the above Equations (1) and (2) proceed at a high current density condition, pH in the vicinity of cathode will rise due to the hydrogen evolution as a side reaction of electrodeposition. In the present study, pH in the bulk solution is 3.0 as described in the experimental section. Hence, at a high current density condition, pH in the vicinity of cathode will rise up to 6.5 and more. $Cu_4(OH)_6SO_4$ will be formed in the pH range more than 4 according to the potential-pH diagram of the $CuSO_4$-H_2O system [36]. In the same way, Cu_2O will also be precipitated in the pH range more than 4 on the basis of the potential-pH diagram of the Cu-H_2O system [37]. Therefore, it seems that the hydroxide (i.e., $Cu(OH)_2$) or cuprous oxide (i.e., Cu_2O) could be included into the electrodeposited Cu films because the oxygen bridge in the PEG molecule can adsorb on the surface of the Cu cathode as well as Cu_2O crystallites [38]. Zhang et al. reported that the PEG network on the surface of the Cu cathode reduces the nucleation points on the cathode and isolates the initial crystallites from aggregating. Hence, the dispersity of Cu_2O crystallites on the cathode will be greatly improved [38]. These PEG effects will accelerate the electrochemical reactions as described in the above Equations (1) and (2). Therefore, in the present study, PEG seems to act as a depolarizer, as shown in Figure 1.

By the way, as shown in Figure 1, the slope of the cathodic polarization curve decreased by shifting the potential to a region that is in a range from −0.4 V to −1.4 V vs. Ag/AgCl due to the decrease in Cu^{2+} ion concentrations in the vicinity of the cathode. In the potential range, the cathode current density is more than ca. 1000 A/m^2 and the rate-limiting process will be the mass transfer such as the migration of Cu^{2+} ions. In contrast, in the potential region that is in a range from +0.1 V to −0.4 V vs. Ag/AgCl, the rate-limiting process will be the charge transfer of Cu^{2+} ions. Hence, in this study, the cathode current density for electrodeposition was set to 900 A/m^2 to improve both the productivity and surface smoothness of metallic copper or Cu/Cu_2O dual phase composite films.

3.2. Structure of Electrodeposited Cu and Cu_2O Dual Phase Composite Films

Figure 2 shows the effect of PEG concentration ((a): 0 gL^{-1}, (b): 0.01 gL^{-1}, (c): 0.02 gL^{-1}, (d): 0.03 gL^{-1}, (e): 0.04 gL^{-1}, (f): 0.05 gL^{-1}) on the XRD profiles of electrodeposited Cu and Cu_2O dual phase composite films. The diffraction peaks derived from fcc-Cu (111) and (220) were observed in all samples. In addition to these peaks that derived from a metallic copper phase, the peaks derived from a copper oxide phase were also observed in the samples which were obtained from the solution containing PEG (Figure 2(b)–(f)). In the metallic copper thick film that was electrodeposited from the solution without PEG (Figure 2(a)), the preferential crystal orientation in fcc-Cu (220) was observed, as shown in Figure 2. This tendency corresponds well to the results reported by Rasmussen et al. [39]. By contrast, in the Cu and Cu_2O dual phase composite films that were electrodeposited from the solutions containing PEG (Figure 2(b)–(f)), the preferential crystal orientation in fcc-Cu (220) was diminished, while that in fcc-Cu (111) was enhanced and the random crystallographic orientation was observed. This drastic change in crystal orientation seems to be caused by the PEG adsorption effect on the cathode where the electrochemical reduction process and the crystal growth process for the electrodeposited metallic copper are suppressed. This reduction in the copper growth rate induces the preferential crystal orientation in fcc-Cu (111), which corresponds to the closest packed plane in fcc. This tendency corresponds well to the results that were investigated on the transformation of crystal orientation to the (111) plane with increasing the solution pH reported by Wang et al. [28]. Furthermore, in the samples which were electrodeposited from the solutions containing PEG (Figure 2(b)–(f)), the preferential crystal orientation in Cu_2O (200) was also observed. Zhou et al. reported that the preferential crystal orientation in electrode-

posited Cu_2O films was strongly affected by electrolysis conditions such as the solution pH and cathode potential [27]. They revealed that the preferential crystal orientation in Cu_2O (200) emerged in the samples which were obtained in the solution pH range less than 10 and in the cathode potential range that was nobler than −0.4 V vs. SCE. On the contrary, they also founded that the diffraction peak which derived from Cu_2O (111) was also detected and the preferential crystal orientation was altered to a random state in the samples which were obtained in the solution pH range more than 10 and in the cathode potential range that was less noble than −0.4 V vs. SCE. In the present study, with increasing the PEG concentration up to 0.05 g/L, the diffraction peak which derived from Cu_2O (111) was also detected, as shown in Figure 2(f). Hence, PEG seems to improve the dispersity of Cu_2O crystallites and make a random crystal orientation.

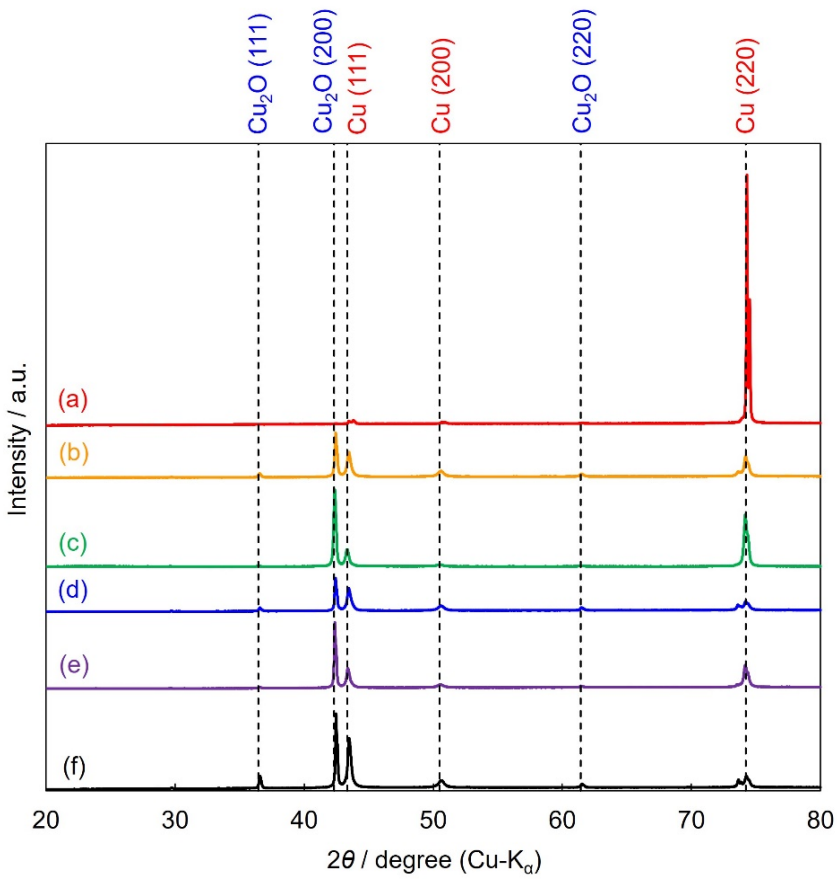

Figure 2. Effect of PEG concentration ((a): 0 gL^{-1}, (b): 0.01 gL^{-1}, (c): 0.02 gL^{-1}, (d): 0.03 gL^{-1}, (e): 0.04 gL^{-1}, (f): 0.05 gL^{-1}) on the XRD profiles of electrodeposited Cu and Cu_2O dual phase composite films.

Figure 3 shows the effect of PEG concentration ((a): 0 gL^{-1}, (b): 0.01 gL^{-1}, (c): 0.02 gL^{-1}, (d): 0.03 gL^{-1}, (e): 0.04 gL^{-1}, (f): 0.05 gL^{-1}) on the surface appearance (optical microscope images) of electrodeposited Cu and Cu_2O dual phase composite films. As shown in Figure 3a, the surface appearance (optical microscope images) of copper film electrodeposited from the solution without PEG showed a red-orange color with a metallic luster characteristic of a typical metallic copper. By contrast, the addition of PEG caused the surface to turn black due to precipitating the copper oxide phase (Figure 3b–f). This tendency corresponds well to the results reported by Rahman et al. [40]. The above phenomenon may be attributed to the inhibition of pH buffering effect of H_3BO_3 by adsorption of PEG on the cathode, which results in a rapid increase in pH near the cathode. According to the potential-pH diagram of the Cu^{2+}-H_2O system [41], copper oxide can be deposited via copper hydroxide which will be formed on the cathode when the pH increases in the

vicinity of the cathode. Therefore, it was estimated that Cu and Cu_2O dual phase composite films could be prepared by adding PEG.

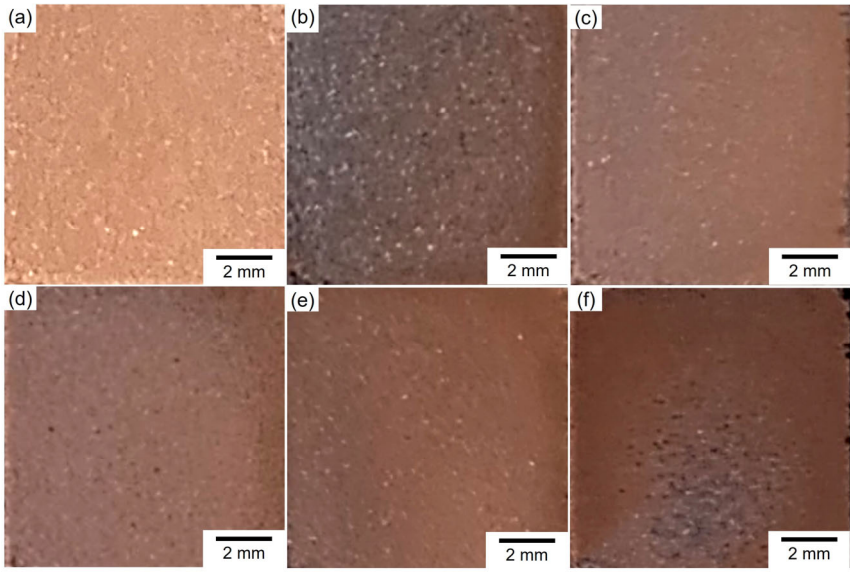

Figure 3. Effect of PEG concentration ((**a**): 0 gL^{-1}, (**b**): 0.01 gL^{-1}, (**c**): 0.02 gL^{-1}, (**d**): 0.03 gL^{-1}, (**e**): 0.04 gL^{-1}, (**f**): 0.05 gL^{-1}) on the surface appearance (optical microscope images) of electrodeposited Cu and Cu_2O dual phase composite films.

Figure 4 shows the effect of PEG concentration ((a): 0 gL^{-1}, (b): 0.01 gL^{-1}, (c): 0.02 gL^{-1}, (d): 0.03 gL^{-1}, (e): 0.04 gL^{-1}, (f): 0.05 gL^{-1}) on the SEM images of electrodeposited Cu and Cu_2O dual phase composite films. As shown in Figure 4a, the morphology of the composite film, which was electrodeposited from the solution without PEG, exhibited a coarse structure with large crystal grains. By contrast, in the solution containing PEG, the surface morphology was transformed to exhibit a smooth appearance with fine crystal grains (Figure 4b–f). This improvement in the surface appearance seems to have been caused by PEG adsorption on the cathode to suppress the heterogeneous nucleation of electrochemically reduced metallic copper atoms.

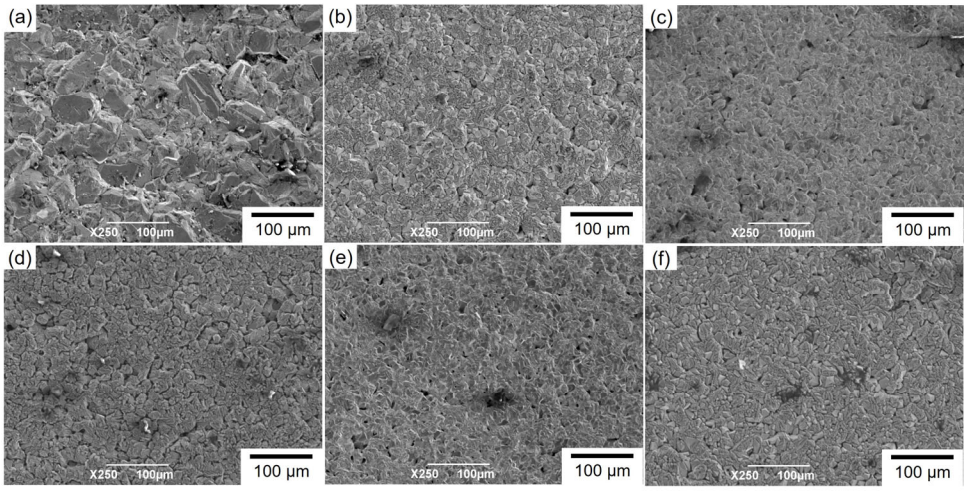

Figure 4. Effect of PEG concentration ((**a**): 0 gL^{-1}, (**b**): 0.01 gL^{-1}, (**c**): 0.02 gL^{-1}, (**d**): 0.03 gL^{-1}, (**e**): 0.04 gL^{-1}, (**f**): 0.05 gL^{-1}) on the SEM images of electrodeposited Cu and Cu_2O dual phase composite films.

Figure 5 shows the effect of PEG concentration on the surface roughness R_a of electrodeposited Cu and Cu_2O dual phase composite films. The surface roughness was approx-

imately 6 μm in the sample that was electrodeposited from an aqueous solution without PEG. By contrast, the addition of PEG significantly reduced the surface roughness to less than 4 μm. This result is consistent with the tendency of surface appearance of electrodeposited Cu and Cu_2O dual phase composite films, as shown in Figure 3. Therefore, the effect of PEG addition on the morphology of the composite films seems to be quite sensitive even at very small amounts.

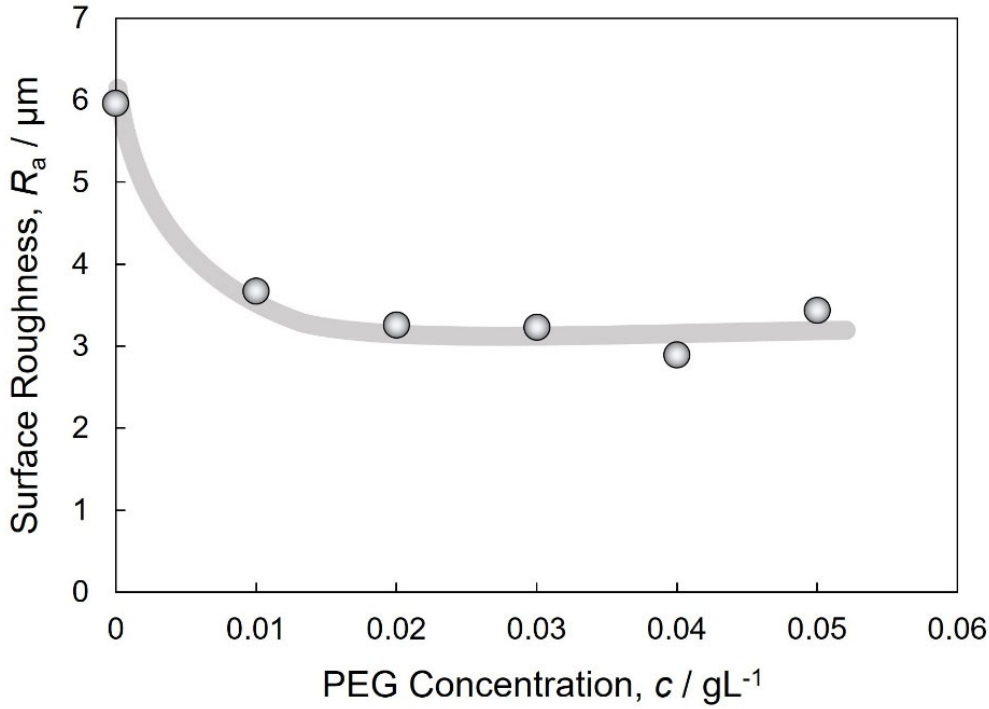

Figure 5. Effect of PEG concentration on the surface roughness of electrodeposited Cu and Cu_2O dual phase composite films.

Figure 6 shows the effect of PEG concentration on the crystallite size of electrodeposited Cu and Cu_2O dual phase composite films. The average crystallite size d of the electrodeposited Cu and Cu_2O dual phase composite films was determined using the following Equation (3) (Scherrer's formula) [42]:

$$d = \frac{K\lambda}{\beta\, cos\theta} \tag{3}$$

where K, λ and β correspond to the Scherrer's constant (0.94), X-ray wavelength ($Cu - K_\alpha$ = 0.15418 nm) and half width of diffraction peaks, respectively. As shown in Figure 6, the average crystallite size of metallic copper thick film that was electrodeposited from the solution without PEG was approximately 105 nm. By contrast, the average crystallite size of Cu and Cu_2O dual phase composite films that were electrodeposited from the solutions containing PEG was decreased to about 40 nm. This tendency corresponds well to the results that were found on the effect of thiourea as an additive reported by Kumar et al. [43]. This decrease in crystallite size also seems to be induced by the PEG adsorption effect on the cathode that suppresses the crystal growth process of electrodeposited metallic copper, as shown in Figure 4. As shown in Figure 6, in the PEG concentration range above 0.01 g/L, there was not a significant decrease in crystallite size. Therefore, the PEG adsorption effect on the cathode seems to be effective even in a quite small PEG concentration range (only 0.01 g/L).

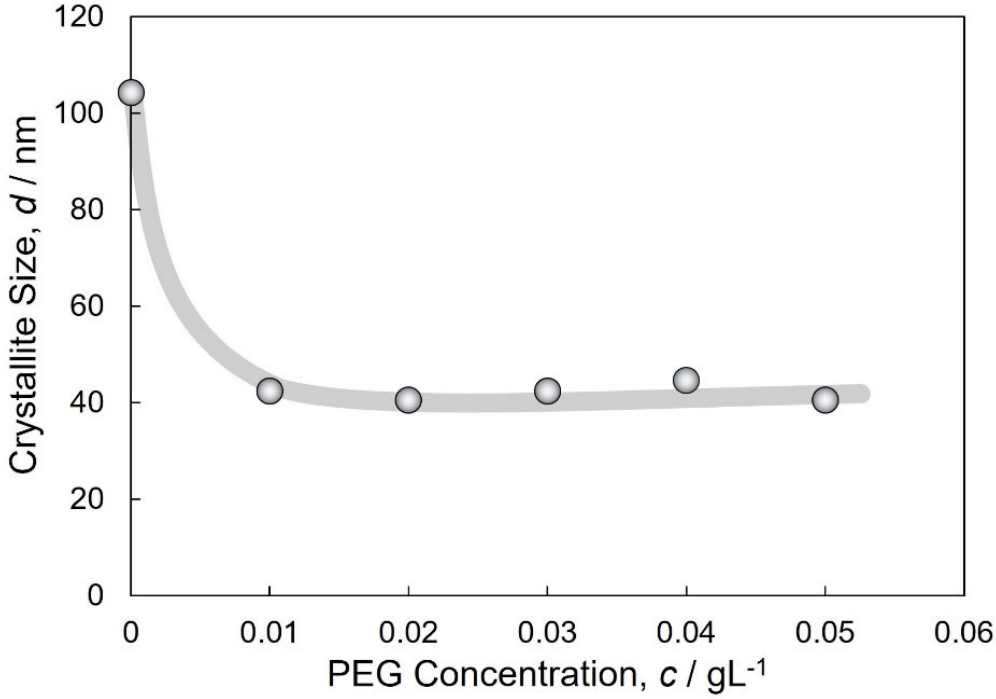

Figure 6. Effect of PEG concentration on the crystallite size of electrodeposited Cu and Cu_2O dual phase composite films.

3.3. Micro-Vickers Hardness of Electrodeposited Cu and Cu_2O Dual Phase Composite Films

Figure 7a shows the effect of PEG concentration on the micro-Vickers hardness of electrodeposited Cu and Cu_2O dual phase composite films. The hardness was approximately 1.21 GPa in the sample that was electrodeposited from the solution without PEG. By contrast, the hardness increased up to 2.53 GPa in the samples that were electrodeposited from the solutions containing PEG. This hardness value is almost twice that of a casted and rolled copper sheet (about 1.08 GPa). Ibanez et al. reported that the microhardness reached up to around 2.2 GPa for the copper film which was electrodeposited at the current density of 1200 A/m^2 [44]. They conducted the hardness measurement by utilizing an applied load of 1 N that is almost identical to the experimental condition (0.98 N) in the present study.

Figure 7b shows the effect of crystallite size on the micro-Vickers hardness of electrodeposited Cu and Cu_2O dual phase composite films. It is well known that the relationship between yield stress and grain size can be expressed by the following Hall-Petch equation (Equation (4)) [45]:

$$\sigma = \sigma_0 + \mathrm{k}d^{-1/2} \tag{4}$$

where σ, σ_0, k and d correspond to the yield stress, internal stress, sliding constant and crystal grain size, respectively. The micro-Vickers hardness increased with decreasing the crystallite size, as shown in Figure 7b. This tendency follows the above Hall-Petch equation (Equation (4)). The increase in the hardness can be explained by the crystal grain refinement effect, which enhances the grain boundary area and suppresses the movement of dislocations [46]. Hakamada et al. reported the effect of gelatin addition on the micro-Vickers hardness of electrodeposited Cu films [47]. They founded that the hardness was approximately 0.98 GPa) in the sample that was obtained from the solution without gelatin. On the contrary, the hardness increased up to 2.15 GPa in the sample that was obtained from the solution containing 0.05 g/L gelatin. They also revealed that the relationship between the hardness and average crystal grain size followed the above Hall-Petch equation (Equation (4)). Hence, the effect of PEG addition seems to be similar to that of gelatin.

In the present study, the molecular weight of PEG was fixed to 3000 and the concentration was varied up to 0.05 g/L. It is well known that the adsorption ability of PEG, which is dissolved in an aqueous solution, depends on the molecular weight [48–50]. Hence, if we

optimize the molecular weight of PEG as well as the concentration in the aqueous solution, the micro-Vickers hardness of electrodeposited Cu and Cu_2O dual phase composite films will be improved further.

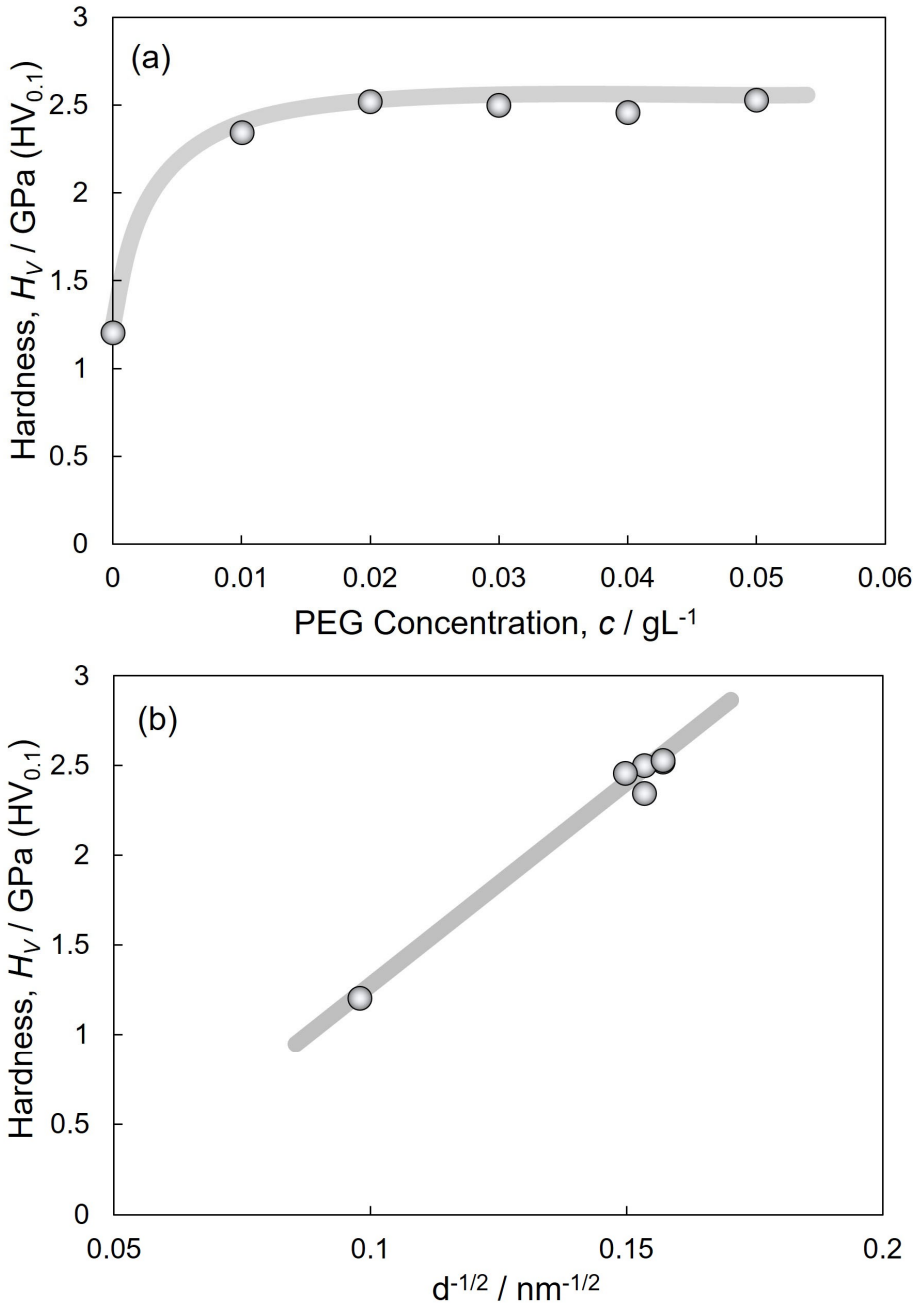

Figure 7. (**a**) Effect of PEG concentration on the micro-Vickers hardness of electrodeposited Cu and Cu_2O dual phase composite films. (**b**) Effect of crystallite size on the micro-Vickers hardness of Cu and Cu_2O dual phase composite films.

4. Conclusions

Polyethylene glycol (PEG) acted as a depolarizer that shifted the cathode potential to the noble direction and decreased the average crystallite size during the electrodeposition of Cu and Cu_2O dual phase composite films. The metallic copper films electrodeposited from the solution without PEG were preferentially orientated in the (220) crystal plane. On the contrary, from the solution containing PEG, Cu and Cu_2O dual phase composite films with random crystal orientation were obtained. The micro-Vickers hardness of the dual phase composite films that were electrodeposited from the solution containing PEG was

achieved up to 2.53 GPa. This improvement in mechanical performance can be explained by the grain refinement effect and the electrochemical phase transformation effect from a copper metallic state to the oxide.

Author Contributions: R.K. and R.S. carried out experiments, analyzed data and wrote the manuscript. S.M. and T.O. designed the study, supervised the project and analyzed data. All authors have read and agreed to the published version of the manuscript.

Funding: This research was funded by Japan Society for the Promotion of Science (JSPS: 18H01754).

Institutional Review Board Statement: Not applicable.

Informed Consent Statement: Not applicable.

Data Availability Statement: Data sets generated during the current study are available from the corresponding author on reasonable request.

Conflicts of Interest: The authors declare no conflict of interest.

References

1. Bai, S.; Liu, J.; Cui, M.; Luo, R.; He, J.; Chen, A. Two-Step Electrodeposition to Fabricate the p-n Heterojunction of a $Cu_2O/BiVO_4$ Photoanode for the Enhancement of Photoelectrochemical Water Splitting. *Dalt. Trans.* **2018**, *47*, 6763–6771. [CrossRef] [PubMed]
2. Khalifa, M.A.; Shen, L.; Zheng, J.; Xu, C. Boosting Light Harvesting and Charge Separation of WO_3 via coupling with Cu_2O/CuO towards Highly Efficient Tandem Photoanodes. *RSC Adv.* **2021**, *11*, 13513–13520. [CrossRef] [PubMed]
3. Kimizuka, N.; Mohri, T. Spinel, $YbFe_2O_4$, and $Yb_2Fe_3O_7$ types of structures for compounds in the In_2O_3 and Sc_2O_3 A_2O_3 BO systems [A: Fe, Ga, or Al; B: Mg, Mn, Fe, Ni, Cu, or Zn] at temperatures over 1000 °C. *J. Solid State Chem.* **1985**, *60*, 382–384. [CrossRef]
4. Nomura, K.; Ohta, H.; Ueda, K.; Kamiya, T.; Hirano, M.; Hosono, H. Thin-film transistor fabricated in single-crystalline transparent oxide semiconductor. *Science* **2003**, *300*, 1269–1272. [CrossRef] [PubMed]
5. Nomura, K.; Ohta, H.; Takagi, A.; Kamiya, T.; Hirano, M.; Hosono, H. Room-temperature fabrication of transparent flexible thin-film transistors using amorphous oxide semiconductors. *Nature* **2004**, *432*, 488–492. [CrossRef] [PubMed]
6. Fan, W.T.; Zhao, Z.Y.; Shen, H.L. Stability and Fundamental Properties of Cu_XO_{1-X} as Optoelectronic Functional Materials. *RSC Adv.* **2022**, *12*, 3755–3762. [CrossRef] [PubMed]
7. Sun, S.; Yang, Q.; Liang, S.; Yang, Z. Hollow Cu_XO (x = 2, 1) Micro/Nanostructures: Synthesis, Fundamental Properties and Applications. *CrystEngComm* **2017**, *19*, 6225–6251. [CrossRef]
8. Shyamal, S.; Hajra, P.; Mandal, H.; Bera, A.; Sariket, D.; Satpati, A.K.; Kundu, S.; Bhattacharya, C. Benign Role of Bi on an Electrodeposited Cu_2O Semiconductor towards Photo-Assisted H_2 Generation from Water. *J. Mater. Chem. A* **2016**, *4*, 9244–9252. [CrossRef]
9. Guo, Y.; Lei, H.; Xiong, L.; Li, B.; Chen, Z.; Wen, J.; Yang, G.; Li, G.; Fang, G. Single Phase, High Hole Mobility Cu_2O Films as an Efficient and Robust Hole Transporting Layer for Organic Solar Cells. *J. Mater. Chem. A* **2017**, *5*, 11055–11062. [CrossRef]
10. Barreca, D.; Comini, E.; Gasparotto, A.; Maccato, C.; Sada, C.; Sberveglieri, G.; Tondello, E. Chemical Vapor Deposition of Copper Oxide Films and Entangled Quasi-1D Nanoarchitectures as Innovative Gas Sensors. *Sens. Actuators B Chem.* **2009**, *141*, 270–275. [CrossRef]
11. Neetzel, C.; Muench, F.; Matsutani, T.; Jaud, J.C.; Broetz, J.; Ohgai, T.; Ensinger, W. Facile Wet-Chemical Synthesis of Differently Shaped Cuprous Oxide Particles and a Thin Film: Effect of Catalyst Morphology on the Glucose Sensing Performance. *Sens. Actuators B Chem.* **2015**, *214*, 189–196. [CrossRef]
12. Al-Jawhari, H.A. A Review of Recent Advances in Transparent P-Type Cu_2O-Based Thin Film Transistors. *Mater. Sci. Semicond. Process.* **2015**, *40*, 241–252. [CrossRef]
13. Xue, J.; Dieckmann, R. The Non-Stoichiometry and the Point Defect Structure of Cuprous Oxide ($Cu_{2-\delta}O$). *J. Phys. Chem. Solids* **1990**, *51*, 1263–1275. [CrossRef]
14. Shimizu, K.; Kobayashi, K.; Thompson, G.E.; Wood, G.C. High Resolution Cross-Sectional Transmission Electron Microscopy of Thermal Oxide Films on Copper. *Corros. Sci.* **1994**, *36*, 621–629. [CrossRef]
15. Reyes-Vallejo, O.; Escorcia-García, J.; Sebastian, P.J. Effect of Complexing Agent and Deposition Time on Structural, Morphological, Optical and Electrical Properties of Cuprous Oxide Thin Films Prepared by Chemical Bath Deposition. *Mater. Sci. Semicond. Process.* **2022**, *138*, 106242. [CrossRef]
16. Chen, Y.J.; Li, M.H.; Huang, J.C.A.; Chen, P. The Cu/Cu_2O Nanocomposite as a p-Type Transparent-Conductive-Oxide for Efficient Bifacial-Illuminated Perovskite Solar Cells. *J. Mater. Chem. C* **2018**, *6*, 6280–6286. [CrossRef]
17. Kamimura, H.; Hayashida, M.; Ohgai, T. CPP-GMR Performance of Electrochemically Synthesized Co/Cu Multilayered Nanowire Arrays with Extremely Large Aspect Ratio. *Nanomaterials* **2020**, *10*, 5. [CrossRef]
18. Saeki, R.; Mizoguchi, S.; Kamimura, H.; Hayashida, M.; Ohgai, T. CPP-GMR Performance of Electrodeposited Metallic Multilayered Nanowires with a Wide Range of Aspect Ratios. *J. Magn. Magn. Mater.* **2021**, *529*, 167849. [CrossRef]

19. Rajeshwar, K. Electrosynthesized Thin Films of Group II–VI Compound Semiconductors, Alloys and Superstructures. *Adv. Mater.* **1992**, *4*, 23–29. [CrossRef]
20. Lincot, D. Electrodeposition of Semiconductors. *Thin Solid Films* **2005**, *487*, 40–48. [CrossRef]
21. Wang, C.; Xu, J.; Shi, S.; Zhang, Y.; Liu, Z.; Zhang, X.; Yin, S.; Li, L. Structural, Optical and Photoelectrical Properties of Cu_2O Films Electrodeposited at Different PH. *RSC Adv.* **2016**, *6*, 4422–4428. [CrossRef]
22. Huang, M.C.; Wang, T.; Chang, W.S.; Lin, J.C.; Wu, C.C.; Chen, I.C.; Peng, K.C.; Lee, S.W. Temperature Dependence on P-Cu_2O Thin Film Electrochemically Deposited onto Copper Substrate. *Appl. Surf. Sci.* **2014**, *301*, 369–377. [CrossRef]
23. Saeki, R.; Ohgai, T. Determination of Cathode Current Efficiency for Electrodeposition of Ferromagnetic Cobalt Nanowire Arrays in Nanochannels with Extremely Large Aspect Ratio. *Results Phys.* **2019**, *15*, 102658. [CrossRef]
24. Sai Guru Srinivasan, S.; Govardhanan, B.; Ashok, M.; Santhosh Kumar, M.C. Influence of Deposition Time on the Visible-Light-Driven Photocatalytic Activity of Cu_2O Thin Films by Reactive Sputtering at Room Temperature. *Mater. Lett.* **2021**, *284*, 128980. [CrossRef]
25. Ismail, W.; El-Shafai, N.M.; El-Shaer, A.; Abdelfatah, M. Impact of Substrate Type on the Surface and Properties of Electrodeposited Cu_2O Nanostructure Films as an Absorber Layer for Solar Cell Applications. *Mater. Sci. Semicond. Process.* **2020**, *120*, 105335. [CrossRef]
26. Li, Q.; Hu, J.; Zhang, J.; Yang, P.; Hu, Y.; An, M. Screening of Electroplating Additive for Improving Throwing Power of Copper Pyrophosphate Bath via Molecular Dynamics Simulation. *Chem. Phys. Lett.* **2020**, *757*, 137848. [CrossRef]
27. Zhou, Y.; Switzer, J.A. Electrochemical Deposition and Microstructure of Copper (I) Oxide Films. *Scr. Mater.* **1998**, *38*, 1731–1738. [CrossRef]
28. Wang, L.C.; de Tacconi, N.R.; Chenthamarakshan, C.R.; Rajeshwar, K.; Tao, M. Electrodeposited Copper Oxide Films: Effect of Bath PH on Grain Orientation and Orientation-Dependent Interfacial Behavior. *Thin Solid Films* **2007**, *515*, 3090–3095. [CrossRef]
29. Ohgai, T.; Hoffer, X.; Gravier, L.; Ansermet, J.-P. Electrochemical Surface Modification of Aluminium Sheets for Application to Nano-Electronic Devices: Anodization Aluminium and Electrodeposition of Cobalt-Copper. *J. Appl. Electrochem.* **2004**, *34*, 1007–1012. [CrossRef]
30. Ohgai, T.; Hjort, K.; Spohr, R.; Neumann, R. Electrodeposition of Cobalt Based Ferro-Magnetic Metal Nanowires in Polycarbonate Films with Cylindrical Nanochannels Fabricated by Heavy-Ion-Track Etching. *J. Appl. Electrochem.* **2008**, *38*, 713–719. [CrossRef]
31. Li, Z.; Soroka, I.L.; Min, F.; Jonsson, M. PH-Control as a Way to Fine-Tune the Cu/Cu_2O Ratio in Radiation Induced Synthesis of Cu_2O Particles. *Dalt. Trans.* **2018**, *47*, 16139–16144. [CrossRef]
32. Oh, Y.-J.; Park, G.-S.; Chung, C.-H. Planarization of Copper Layer for Damascene Interconnection by Electrochemical Polishing in Alkali-Based Solution. *J. Electrochem. Soc.* **2006**, *153*, G617. [CrossRef]
33. Han, J.; Chang, J.; Wei, R.; Ning, X.; Li, J.; Li, Z.; Guo, H.; Yang, Y. Mechanistic Investigation on Tuning the Conductivity Type of Cuprous Oxide (Cu_2O) Thin Films via Deposition Potential. *Int. J. Hydrogen Energy* **2018**, *43*, 13764–13777. [CrossRef]
34. Zeng, T.W.; Yen, S.C. Effects of Additives in an Electrodeposition Bath on the Surface Morphologic Evolution of Electrodeposited Copper. *Int. J. Electrochem. Sci.* **2021**, *16*, 210245. [CrossRef]
35. Hebert, K.R.; Adhikari, S.; Houser, J.E. Chemical Mechanism of Suppression of Copper Electrodeposition by Poly(Ethylene Glycol). *J. Electrochem. Soc.* **2005**, *152*, C324. [CrossRef]
36. Grujicic, D.; Pesic, B. Electrodeposition of copper: The nucleation mechanisms. *Electrochim. Acta* **2002**, *47*, 2901–2912. [CrossRef]
37. Tromans, D.; Sun, R.H. Anodic polarization behavior of copper in aqueous chloride/benzotriazole solutions. *J. Electrochem. Soc.* **1991**, *138*, 3235. [CrossRef]
38. Zhang, Z.; Hu, W.; Zhong, C.; Deng, Y.; Liu, L.; Wu, Y. Preparation of submicron-sized cuprous oxide crystallites by electrodeposition with polyethylene glycol as additive. *J. Cryst. Growth* **2012**, *354*, 193–197. [CrossRef]
39. Rasmussen, A.A.; Jensen, J.A.D.; Horsewell, A.; Somers, M.A.J. Microstructure in Electrodeposited Copper Layers; the Role of the Substrate. *Electrochim. Acta* **2001**, *47*, 67–74. [CrossRef]
40. Sayem Rahman, A.S.M.; Islam, M.A.; Shorowordi, K.M. Electrodeposition and Characterization of Copper Oxide Thin Films for Solar Cell Applications. *Procedia Eng.* **2015**, *105*, 679–685. [CrossRef]
41. Chen, T.; Kitada, A.; Fukami, K.; Murase, K. Determination of Stability Constants of Copper (II)–Lactate Complexes in Cu_2O Electrodeposition Baths by UV-VIS Absorption Spectra Factor Analysis. *J. Electrochem. Soc.* **2019**, *166*, D761. [CrossRef]
42. Saeki, R.; Ohgai, T. Determination of Activation Overpotential during the Nucleation of Hcp-Cobalt Nanowires Synthesized by Potentio-Static Electrochemical Reduction. *Materials* **2018**, *11*, 2355. [CrossRef] [PubMed]
43. Kumar, K.S.; Biswas, K. Effect of Thiourea on Grain Refinement and Defect Structure of the Pulsed Electrodeposited Nanocrystalline Copper. *Surf. Coat. Technol.* **2013**, *214*, 8–18. [CrossRef]
44. Ibanez, A.; Fatas, E. Mechanical and structural properties of electrodeposited copper and their relation with the electrodeposition parameters. *Surf. Coat. Technol.* **2005**, *191*, 7–16. [CrossRef]
45. Bata, V.; Pereloma, E.V. An alternative physical explanation of the Hall–Petch relation. *Acta Mater.* **2004**, *52*, 657–665. [CrossRef]
46. Kumar, K.S.; Van Swygenhoven, H.; Suresh, S. Mechanical Behavior of Nanocrystalline Metals and Alloys. *Acta Mater.* **2003**, *51*, 5743–5774. [CrossRef]
47. Hakamada, M.; Nakamoto, Y.; Matsumoto, H.; Iwasaki, H.; Chen, Y.; Kusuda, H.; Mabuchi, M. Relationship between hardness and grain size in electrodeposited copper films. *Mater. Sci. Eng. A* **2007**, *457*, 120–126. [CrossRef]

48. Dow, W.P.; Yen, M.Y.; Lin, W.B.; Ho, S.W. Influence of molecular weight of polyethylene glycol on microvia filling by copper electroplating. *J. Electrochem. Soc.* **2005**, *152*, C769. [CrossRef]
49. Ko, S.L.; Lin, J.Y.; Wang, Y.Y.; Wan, C.C. Effect of the molecular weight of polyethylene glycol as single additive in copper deposition for interconnect metallization. *Thin Solid Films* **2008**, *516*, 5046–5051. [CrossRef]
50. Song, S.J.; Choi, S.R.; Kim, J.G.; Kim, H.G. Effect of molecular weight of polyethylene glycol on copper electrodeposition in the presence of bis-3-sulfopropyl-disulfide. *Int. J. Electrochem. Sci.* **2016**, *151*, 10067–10079. [CrossRef]